# Electronic structure of Eu and Yb graphite intercalation compounds

S. L. Molodtsov* and C. Laubschat
*Institut für Oberflächen- und Mikrostrukturphysik, Technische Universität Dresden, Mommsenstrasse 13, D-01062 Dresden, Germany*

M. Richter
*Max-Planck-Arbeitsgruppe ''Elektronensysteme,'' Technische Universität Dresden, Mommsenstrasse 13, D-01062 Dresden, Germany*

Th. Gantz
*Institut für Oberflächen- und Mikrostrukturphysik, Technische Universität Dresden, Mommsenstrasse 13, D-01062 Dresden, Germany*

A. M. Shikin
*Institute of Physics, St. Petersburg State University, 198904 St. Petersburg, Russia*
(Received 18 December 1995)

An angle-resolved photoemission (PE) study is performed on graphite intercalation compounds (GIC's) with Eu and Yb prepared *in situ* by deposition of the pure metals onto single-crystalline graphite(0001) surfaces and subsequent annealing. The low-energy-electron-diffraction patterns reveal a sharp $(\sqrt{3}\times\sqrt{3})R30°$ overstructure as observed for other rare-earth (RE) and alkali GIC's. The PE data are in excellent agreement with local-density-approximation band-structure calculations for stage-2 GIC's that indicate charge transfer of about 0.5 electrons per RE atom into graphite-derived states of $\pi$ symmetry. This charge transfer is caused by an energetical lowering of the graphite-derived $\pi$ bands and leads to the appearance of an intense Fermi-level structure in the PE spectra taken around the $K(\Gamma')$ point of the Brillouin zone. Admixtures of rare-earth-derived $d$ states are found close to the Fermi energy in the region of the $\Gamma$ and the $M'$ points. [S0163-1829(96)07424-3]

## I. INTRODUCTION

Graphite intercalation compounds (GIC's) have attracted considerable interest due to their layered, quasi-two-dimensional structure and the resulting large anisotropy of their electric and electronic properties:[1–3] While perpendicular to the atomic planes, the electric conductivity is small and the compounds behave like semiconductors; the conductivity increases primarily in directions parallel to the layers and reaches values close to those of noble metals; additionally, some GIC's become superconducting at low temperatures.[4] The electronic structure of these materials has been widely discussed in various experimental[5–14] and theoretical[15,16] studies. Thereby, electron spectroscopic studies have mostly focused on alkali and alkali-earth-derived GIC's, which can easily be prepared *in situ* under ultra-high-vacuum conditions.

Recently, a series of photoemission (PE) and Auger studies has also been published on GIC's based on the lightest rare-earth (RE) element, lanthanum.[17–20] From a technological point of view, rare-earth compounds are generally interesting due to their magnetic properties and their possible application as magnetic storage materials. In the case of RE-based GIC's, there has also been strong interest in a comparison of their electronic properties with those of alkali-derived GIC's, particularly concerning effects related to the influence of $d$-symmetry orbitals to bonding. Surprisingly, the photoemission studies revealed an almost identical behavior of both types of compounds: as compared to graphite, the general shape of the carbon-derived spectroscopic structures remained unaffected, but the bands were shifted to higher binding energies (BE).[17,20] Within a rigid-band model, this effect was attributed to charge transfer from the metal to unoccupied graphite-derived states. Why the amount of charge transfer is apparently of the same order of magnitude in alkali and La GIC's and whether, particularly for La GIC, the application of a simple rigid-band model can be justified is still not clear. Further problems concern (i) the character of the carbon-derived states that serve as electron acceptors, (ii) the effect of the particular stage of intercalation on the electronic structure of GIC's, and (iii) the question of what happens to the RE-$5d^1$ state upon bonding.

In the present paper, we report on a photoemission study of single-crystalline Eu and Yb GIC's prepared *in situ* by evaporation of the pure rare-earth metals on graphite(0001) and subsequent annealing. In contrast to La, Eu and Yb are divalent metals with unoccupied $d$ states located immediately above the Fermi energy ($E_F$). In order to study the influence of these states on bonding, local-density-approximation (LDA) band-structure calculations employing a method of optimized linear combination of atomic orbitals (LCAO) have been performed for different structural arrangements. The obtained results were compared to the photoemission data. Perfect agreement between theory and experiment was obtained when a stage-2 intercalation was assumed.

In analogy to GIC's of alkalies, alkali-earth metals, and La, the bonding in Eu and Yb GIC's is almost ionic, characterized by a charge transfer of about 0.5 electrons from each Eu or Yb atom into unoccupied graphite-derived states of $\pi$ symmetry instead of the ''interlayer band,''[21] which, according to our calculations, lies clearly above the Fermi en-

 

ergy in these intercalation compounds. As in the case of other GIC's, the charge transfer is caused by an energetic lowering of all $\pi$-symmetry graphite-derived bands. A description within a rigid-band model fails, however, to predict the behavior of the $\sigma$ states as well as details of the electron band structure close to $E_F$. The RE-derived $d$-like states are found close to the $M'$ point in the Brillouin zone (BZ) of Eu and Yb GIC's, in agreement with a previous resonant PE study on La GIC.[20]

## II. EXPERIMENTAL DETAILS

Single-crystalline flakes of natural graphite with typical diameters of 7–9 mm were cleaved with an adhesive tape and subsequently carefully degassed *in situ* during several hours at a temperature of $\cong$1700 K in a vacuum better than $3\times10^{-10}$ mbar. Clean surfaces reveal the characteristic hexagonal low-energy-electron-diffraction (LEED) pattern of graphite(0001).

Similar to our previous work on La GIC,[17–20] the *in situ* intercalation of Eu and Yb into the graphite matrix was performed by thermal deposition of relatively thick layers of RE ($\cong$100 Å) onto the clean graphite surface followed by step-by-step annealing of the system at increasing temperatures. Deposition of RE's was performed at rates of 3–5 Å /min by means of a simple resistively heated evaporator consisting of metallic drops placed inside of *W*-RE coils. Drops of Eu and Yb were prepared in Ar atmosphere by melting of small pieces of 99.999% purified Re ingots (from Goodfellow, Inc.) in order to reduce possible bulk contaminations. The thickness of the deposited Eu and Yb films was monitored by a quartz microbalance. The vacuum during evaporation was in the range of $4\times10^{-10}$ mbar. Deposition of 100-Å-thick layers of RE's onto graphite at room temperature resulted in nonordered interfaces terminated by the pure metals at the surface. Several stages of annealing of the Eu/graphite (Yb/graphite) interfaces with increasing temperatures from 600 to 1000 K (from 600 to 800 K) with intervals of 100 K and annealing periods of 5 min each led to a recovering of periodic structures. Both Eu/graphite and Yb/graphite interfaces give $(\sqrt{3}\times\sqrt{3})R30°$ reconstructed LEED patterns.

The experiments were performed at the Berliner Elektronenspeicherring für Synchrotronstrahlung (BESSY) using the TGM1 beamline. Angle-resolved valence-band photoemission spectra were taken at photon energies of 33 and 50 eV with a hemispherical electron-energy analyzer (ARIES, Vacuum Science Workshop, Ltd.) tuned to an energy resolution of 150 meV [full width at half maximum (FWHM)] and an angle resolution of 1°. The photon incidence angle was selected to be 35° relative to the sample surfaces in order to monitor bands of both $\pi$ and $\sigma$ symmetry. The basic pressure during measurements was always lower than $1\times10^{-10}$ mbar.

## III. BAND STRUCTURE CALCULATIONS

Electronic structure calculations were carried out in the framework of LDA using the Hedin-Lundqvist exchange-correlation potential.[22] The GIC's were treated as ideal crystalline structures; no account was taken of surface and real structure effects. A number of different stacking sequences were considered, since the correct sequence could not be directly extracted from the available experimental data. In particular, for Eu [-RE-C-] (stage-1 GIC); [-RE-C-RE-C-C-]; [-RE-C-RE-C-C-C-]; [-RE-C-C-] (stage-2 GIC); and [-RE-C-C-C-] (stage-3 GIC) sequences were considered. In the case of Yb, calculations were only done for the first- and the second-stage intercalation compounds. Due to the considerable size of the elementary cells (7–26 atoms), the use of a minimum basis scheme (i.e., the size of the Hamiltonian matrix equals the number of valence electrons per unit cell) was desirable. We employed the method of optimized linear combination of atomic orbitals[23] in its scalar relativistic version.[24] The set of atomic orbitals included the RE $5d$, $6s$, and $6p$ states as well as the C $2s$ and $2p$ states. The $4f$ electrons were assumed to be localized, making up a divalent configuration ($4f^7$ and $4f^{14}$ for Eu and Yb, respectively). This behavior was simulated by treating the $4f$'s as core states. The **k** sums were carried out using the linear tetrahedron method at a mesh of 38 to 114 **k** points in the irreducible part of the Brillouin zone.

TABLE I. Characteristic binding energies (in eV relative to $E_F$) for the valence bands of graphite from full-potential linearized-augmented-plane-wave (FLAPW Ref. 25), full-potential linear-muffin-tin-orbital (FPLMTO Ref. 26), and present (LCAO) calculations in comparison to experimental data from Refs. 5, 27, and 28 and the present study.

| | Theory | | | Experiment | | | |
|---|---|---|---|---|---|---|---|
| State | FLAPW[a] | FPLMTO[b] | LCAO | [c] | [d] | [e] | Present |
| Bottom $\pi$ | 8.7 | 7.8 | 8.6 | 8.1 | 8.5 | | 8.4 |
| | 6.7 | 6.4 | 6.0 | 7.2 | 6.6 | 5.7 | 7.1 |
| Bottom $\sigma$ | 19.6 | 19.2 | 18.2 | 20.6 | | | 21.5 |
| | 19.3 | | 17.4 | | | | |
| Top $\sigma$ | 4.6 | 3.4 | 3.1 | 4.6 | 5.5 | | 4.3 |

[a]Jansen and Freeman (Ref. 25).
[b]Ahuja *et al.* (Ref. 26).
[c]Eberhardt *et al.* (Ref. 5).
[d]Law *et al.* (Ref. 27).
[e]Bianconi *et al.* (Ref. 28).

As a first step, calculations were performed for pure hexagonal graphite (space group $P6_3/mmc$, $a=4.656$ a.u., $c=12.682$ a.u.). The obtained energies at the $\Gamma$ point of the BZ are compared in Table I with the results of two recent high-precision LDA calculations,[25,26] experimental data from the literature, and our own PE experiments. Our data calculated for $\pi$ states lay within the scatter of the experimental values. In the case of the $\sigma$-symmetry bands, however, notable deviations were obtained between the results of our calculations and the data presented in literature as well as those measured in the present study. The eigenstates of the $\sigma$-symmetry bands are more sensitive to details of the potential construction, which is somewhat less accurate in our calculations than in the full-potential schemes used in Refs. 25 and 26. On the other hand, a difference of 1–2 eV remains even between these more exact calculations and experimental results.

In order to exclude systematic deviations between theory and experiment, we adjusted the top of the $\sigma$ band to our measured value. Technically, this was achieved by shifting

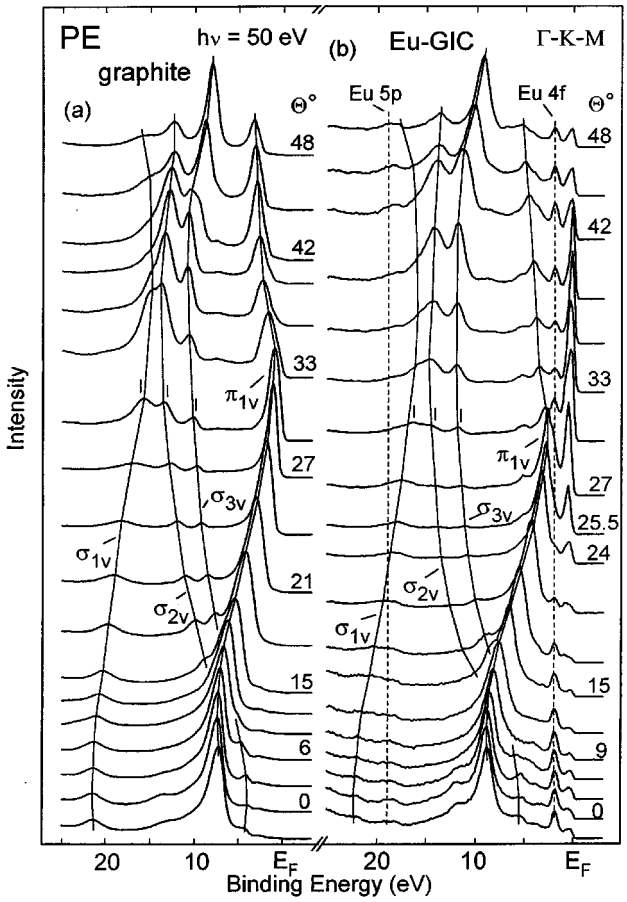


FIG. 1. EDC's of pristine graphite (a) and Eu GIC (b) taken at 50 eV photon energy along the Γ-*K*-*M* direction. The two sets of PE spectra were measured at various Θ's (from −3° to 48°) with increments of 3°. In addition, a spectrum of Eu GIC recorded at Θ=25.5° is shown in the right-hand panel.

the carbon $2p_x$ and $2p_y$ diagonal Hamiltonian matrix elements by −1.2 eV in all further calculations. Thereby, it was assumed (and proved *a posteriori*) that the carbon $\sigma$ orbitals do not hybridize to the RE states. Upon this assumption, an application of the same correction to all investigated structures seems to be justified. In the following, the calculated bands for Eu and Yb GIC's will be discussed in comparison to the experimental data and the electronic structure of pristine graphite.

## IV. RESULTS

### A. Electronic structure of Eu GIC: Comparison to pristine graphite

Two sets of PE spectra for pristine graphite and Eu GIC taken at a photon energy of 50 eV at various polar angles Θ are shown in Figs. 1(a) and 1(b), respectively. In this way, changing only the polar angle, we scanned the band structure along the Γ-*K* direction in the first BZ as well as along the *K*-*M* direction in the second BZ of graphite. The spectra are normalized each to its maximal intensity. Solid lines through the peaks serve as guides to the eyes indicating tentative band dispersions in the figure. The energy-distribution curves (EDC's) measured for pristine graphite at both $h\nu=50$ eV and $h\nu=33$ eV (not shown) are in accordance with data reported in previous PE studies.[5,27,28] The spectra are characterized by four main bands, which clearly can be monitored with 50-eV photons. At small angles the $\pi_{1v}$ symmetry band originating from the $C\ 2p_z$ orbitals reveals the highest PE intensity; it disperses toward the Fermi level in the first Brillouin zone and comes down to higher binding energies at larger polar angles. This band reaches $E_F$ close to the *K* point ($\Theta\cong30°$) that is the only region in the reciprocal space of graphite with nonzero density of states at the Fermi level.[25,26] The PE weight of this band drops in the second BZ, an effect that can be explained by the change in sign of the reduced **k** vector in the initial state, whereas the momentum of the free-electron-like final state continues smoothly across the BZ boundary.[29]

The other three bands of graphite marked in Fig. 1(a) give a $\sigma$ symmetry. Two of them, which have $2p_{x,y}$ character, are degenerated at the Γ point at about 4.3 eV binding energy. These bands disperse toward higher BE's when going away from the center of the Brillouin zone. They cross the $\pi_{1v}$ band in the region of $9°<\Theta<12°$ giving no rise to hybridization phenomena. For polar angles $\Theta>15°$ these bands are energetically split into high-BE ($\sigma_{2v}$) and low-BE ($\sigma_{3v}$) components. Close to the border of the BZ the $2p_{x,y}$-originated bands converge with the $2s$-derived band ($\sigma_{1v}$ symmetry), which is located at 21.5 eV at the Γ point. The energy overlap between these bands leads to the formation of the $sp^2$ hybrids characteristic for the well known structure of the hexagonally arranged graphite layers. The PE intensities of all three $\sigma$-symmetry bands grow in the second BZ as compared to the weight of the $\pi$-character band as expected for emissions from $\pi$- and $\sigma$-type orbitals.[30]

The angle-resolved EDC's of Eu GIC shown in Fig. 1(b) are very similar to the PE spectra of graphite. They display all four bands ($\pi_{1v}$ and $\sigma_{1v-3v}$) present also in Fig. 1(a). In Eu GIC, however, these bands are shifted by 0.3–1.7 eV toward higher BE's, depending on their symmetry and the point monitored in the BZ of the intercalation compound. As a general trend, the $\sigma$-symmetry bands are less shifted than the $\pi$-symmetry states. In particular, the $\sigma_{1v}$ band moves by only 0.6 eV, while the $\pi_{1v}$ band is shifted by 1.6 eV at the Γ point. The triplet structure observed in the region of the $sp^2$ hybrid bonds in pristine graphite (marked by vertical ticks) is preserved in the PE spectra of the GIC. In addition to these four graphite-derived bands, a new intense feature appears within the first 1.5 eV below the Fermi level. This Fermi-energy structure is present at all Θ's, while its intensity is strongly modulated with the angle of analyzing. Maximal PE intensity of this feature, which is comparable to the large PE signal from the $\pi_{1v}$ band for $\Theta<27°$, was measured in the range of $27°<\Theta<39°$ that corresponds to the region around the *K* point of the Brillouin zone of pristine graphite. Its minimal intensity was observed for polar angles between 9° and 21°. The weight of the Fermi-energy structure slightly increases again close to the Γ point.

Besides the valence bands discussed above, other structures assigned to Eu-originated states (marked by broken vertical lines) are present in the PE spectra of Eu GIC. The $4f$ emission of Eu represents a peak at 1.9 eV BE, which, as expected, does not show any dispersion over the whole range of polar angle variations. The PE signal related to the Eu $5p$ states is seen at about 19 eV BE.[31] This structure is

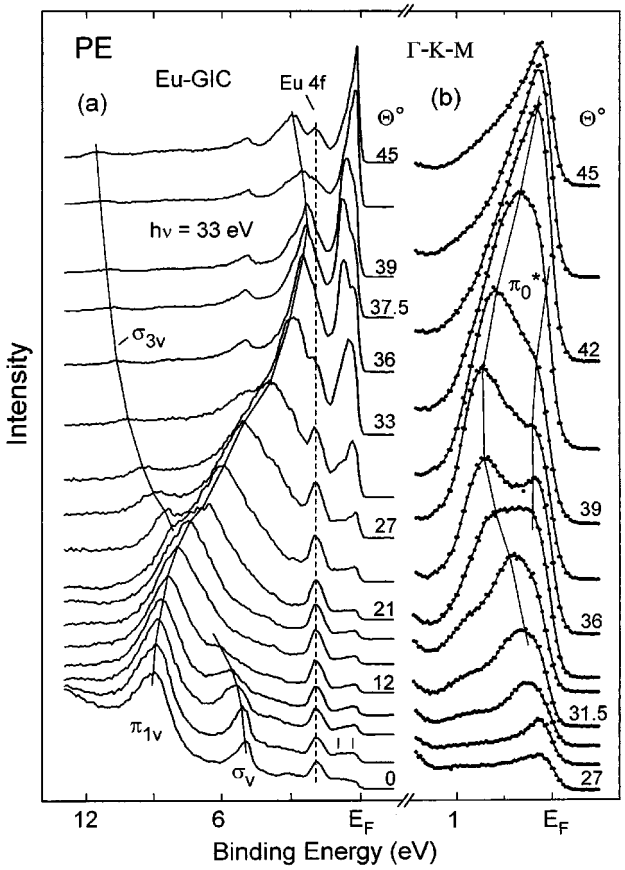


FIG. 2. EDC's of Eu GIC taken at 33 eV photon energy along the Γ-*K*-*M* (Γ-*M*′-Γ′-*M*′) direction at various Θ's: (a) with increments of $\Delta\Theta = 3°$ in a wide energy range. A spectrum recorded at $\Theta = 37.5°$ is also shown in the left-hand panel; (b) with $\Delta\Theta = 1.5°$ in the energy region close to $E_F$ around the $K(\Gamma')$ point.

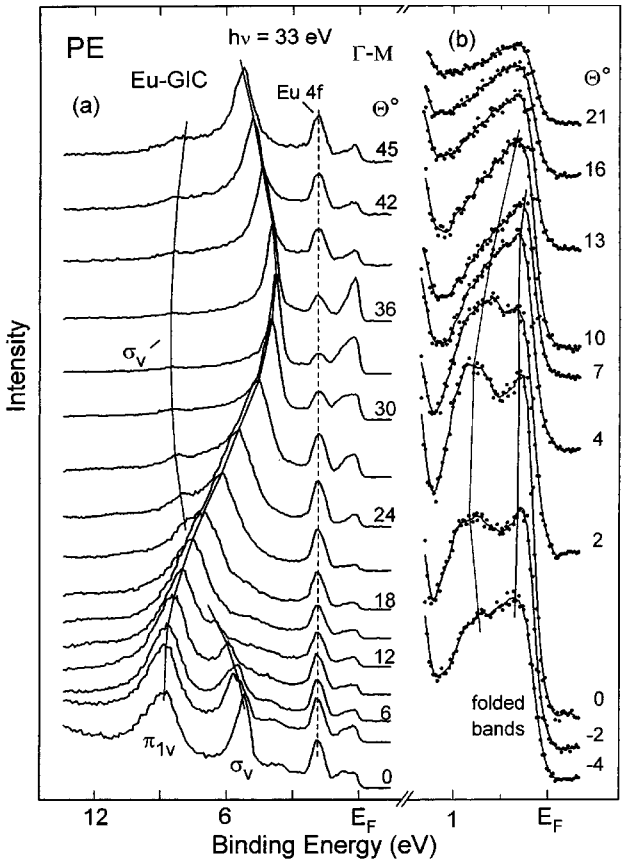


FIG. 3. EDC's of Eu GIC taken at 33 eV photon energy along the Γ-*M* (Γ-*K*′-*M*′) direction at various Θ's: (a) with increments of $\Delta\Theta = 3°$ in a wide energy range; (b) in the energy region close to the Fermi energy.

strongly broadened due to multiplet splitting caused by the coupling of the $5p$ photohole to the open $4f$ shell; it can hardly be analyzed due to its extremely low intensity.

### B. Electronic structure of Eu GIC: Γ-*M*′-Γ′ and Γ-*K*′-*M*′ directions

Intercalation leads to a reconstruction of the Brillouin zone as compared to the maternal BZ of pristine graphite.[13] Therefore, a correct analysis requires one to account for a folding of the electronic bands. The direction Γ-*K*-*M* (Γ-*M*) in the BZ of graphite corresponds to the direction Γ-*M*′-Γ′-*M*′ (Γ-*K*′-*M*′) in the BZ of Eu GIC, as can be derived from the $(\sqrt{3}\times\sqrt{3})R30°$ type of reconstruction of the corresponding LEED pattern.

For a detailed study of the band structure of GIC's we chose low photon energies, which provide better resolution in **k** space as well as high cross sections for graphite-derived $2p$ bands. In Fig. 2(a) we present a series of angle-resolved PE spectra of Eu GIC taken at 33 eV photon energy along the Γ-*K*-*M* (Γ-*M*′-Γ′-*M*′) direction. The structure in the energy region close to $E_F$ measured around the *K* point in the BZ of pristine graphite (corresponds to the Γ′ point in the second BZ of Eu GIC) is shown with an extended scale in Fig. 2(b). In order to stress strong intensity variations, these spectra are normalized to the flux of the incident photons.

As in the experiment with 50-eV photons, the valence-band PE spectra of Eu GIC, taken at $h\nu = 33$ eV along the Γ-*M*′-Γ′-*M*′ direction are dominated by the $\pi$- and $\sigma$-derived bands of graphite. The most intense structure corresponds to the $\pi_{1v}$-derived band that is located at ≅9 eV BE at the Γ point and disperses toward $E_F$, reaching its nearest position relative to the Fermi level close to the Γ′ point ($\Theta \cong 37°$). The $\sigma$-derived electronic states, which are observed at ≅5 eV BE at the Γ point, disperse away from $E_F$ crossing the $\pi_{1v}$ band in the region of the *M*′ point ($\Theta \cong 18°$–$20°$). In contrast to the spectra in Fig. 1(b), the intense Fermi-energy structure measured close to the Γ′ point in Eu GIC [Fig. 2(b)] is split into two bands. The upper band seems to be always cut by the Fermi-edge and appears below $E_F$ only in a narrow range $34.5° < \Theta < 39°$. The lower band reveals stronger dispersion: It crosses the Fermi level from both sides of the Γ′ point at $\Theta \cong 31.5°$ and 42° and approaches the $\pi_{1v}$-derived band at $\Theta \cong 37°$. The two latter bands, however, do not cross each other. Instead, they are separated by a gap of ≅1.5 eV in the region close to the Γ′ point.

The PE intensity in the Fermi-energy region drops on the way from the Γ′ to the Γ point when the dispersive band discussed above intersects $E_F$ at $\Theta \cong 31.5°$. The EDC's mea-

sured at $9°<\Theta<23°$ [Fig. 2(a)] reveal a trianglelike shape in the energy region within the first 1.5 eV below $E_F$; additionally, a weak shoulder seems to be present at $\cong 0.8$ eV BE. Note, that this shoulder is more pronounced in the range of $\Theta$'s between 23° and 33°. The PE weight in the Fermi-energy region increases slightly again close to the $\Gamma$ point. A tiny structure can be distinguished in normal-emission spectra close to $E_F$ [marked by vertical ticks in Fig. 2(a)]. Further relatively weak structures are observed in the energy range of 2.5–4.5 eV BE. The nondispersive $4f$ emission of Eu is indicated by a vertical dashed line.

PE spectra of Eu GIC measured in a wide binding-energy range along the $\Gamma$-$M$ ($\Gamma$-$K'$-$M'$) direction are presented in Fig. 3(a). The spectral region close to the Fermi-energy is shown with an extended scale in Fig. 3(b). As in the case of the $\Gamma$-$M'$-$\Gamma'$-$M'$ direction, the electronic structure along the $\Gamma$-$K'$-$M'$ direction is caused mainly by the $\pi$- and $\sigma$-graphite-derived bands [Fig. 3(a)]. An intense PE weight of the $\pi_{1v}$ band is observed for all polar angles. Similar to the $\Gamma$-$M'$-$\Gamma'$-$M'$ direction, this band disperses toward the Fermi level, reaching its nearest position to $E_F$ at the zone boundary of the nonreconstructed BZ (the $M$ point corresponds to the $M'$ point). It disperses back to higher binding energies for $\Theta>36°$. The $\sigma$-derived band diverges first toward higher BE's and then moves (beginning from $\Theta\cong 40°$) back to the Fermi level.

The emission intensity close to the Fermi energy changes with $\Theta$ and becomes maximal in the range of $\Theta$'s between 30° and 39°. It drops for smaller polar angles and grows again around the $\Gamma$ point. In contrast to the EDC's presented in Fig. 2, the PE weight close to $E_F$ measured in the region of the border of the nonreconstructed BZ ($\Theta\cong 33°$, $M$ point) has a trianglelike line shape; the signal here is not as intense as in Fig. 2(b). Around the $\Gamma$ point, the PE spectra reveal two well resolved structures, which behave very similarly to those observed around the $K$ point [$31.5°<\Theta<42°$, Fig. 2(b)]. Note the much higher intensity of the structure close to the $K$ point of the nonreconstructed BZ. Since in the BZ of the Eu GIC this point is equivalent to the $\Gamma'$ point, we assign the structure in the PE spectra measured close to normal emission [Fig. 3(b)] to back-folded bands originating at the $K$ point. This assignment is in accordance to the observation that PE intensities of folded bands in GIC's are normally much lower compared to signals from unfolded bands.[5,7]

### C. Electronic bands of Yb GIC in comparison to electronic structure of Eu GIC

The PE spectra of Yb GIC measured with 33-eV photons along the $\Gamma$-$K$-$M$ ($\Gamma$-$M'$-$\Gamma'$-$M'$) direction are shown in Fig. 4(a). There are almost no differences between Yb and Eu GIC's in the electronic structure of both the $\pi_v$- and the $\sigma_v$-graphite-derived bands [compare Figs. 2(a) and 4(a)]. Similarly to Eu GIC a new structure appears in the Fermi-energy region in the PE spectra of Yb GIC. In the same way as in Fig. 2(a), the weight of this structure is modulated over the whole range of polar angles. However, at variance to Eu GIC, where this structure is split into two nearly equally intense bands close to the $K$ point [Fig. 2(b)], the Fermi-energy feature in the EDC's of Yb GIC measured in the corresponding range of angles $33°<\Theta<42°$ represents an

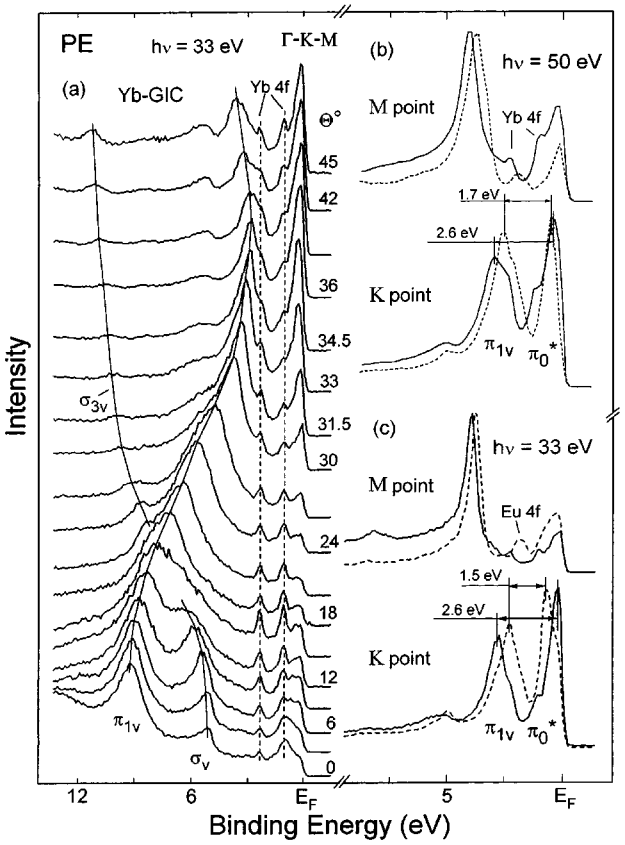


FIG. 4. (a) EDC's of Yb GIC taken at 33 eV photon energy along the $\Gamma$-$K$-$M$ ($\Gamma$-$M'$-$\Gamma'$-$M'$) direction at various $\Theta$'s (from 0° to 45°) with $\Delta\Theta=3°$. Two further spectra recorded at $\Theta=31.5°$ and $\Theta=34.5°$ are also shown in the left-hand panel. (b) and (c) represent a comparison between PE spectra of Eu GIC (broken lines) and Yb GIC (solid lines) measured at both the $K$ and the $M$ points with 50-eV and 33-eV photons, respectively.

intense singlet with a rather weak high-BE shoulder. A doublet with two components at 1.1 and 2.3 eV BE originates from the $4f$ emission of Yb.

Figures 4(b) and 4(c) represent PE spectra of Yb and Eu GIC's taken at the $K$ and $M$ points at 50 and 33 eV photon energies, respectively. EDC's measured for Yb GIC are shown by solid lines, while spectra of Eu GIC are illustrated by broken tracks in these figures. Except for the $4f$ multiplets and the line shapes of the Fermi-energy feature at the $K$ point ($h\nu=33$ eV), the corresponding spectra of these two GIC's look qualitatively similar. The structure at $E_F$, however, seems to be systematically shifted toward the Fermi level in Yb as compared to Eu GIC. On the other hand, the $\pi_{1v}$ band lies deeper in Yb GIC. This leads to a wider gap between the two prominent features at the BZ boundaries in Yb GIC.

## V. DISCUSSION

For *in situ* intercalation of the rare earth (Eu and Yb) into single-crystalline graphite we used a method cross-proved in our previous studies of La GIC. Photoelectron diffraction, LEED, resonant, and angle-resolved PE including Fermi surface mapping, Auger-electron spectroscopy, and scanning tunneling microscopy of La GIC (Refs. 17–20 and 32) show

TABLE II. Charge transfer in stage-1 and stage-2 intercalation compounds.

| | $EuC_x$ | | $YbC_x$ | |
|---|---|---|---|---|
| | Eu | C | Yb | C |
| $x=6$ | 0.52 | −0.09 | 0.46 | −0.08 |
| $x=12$ | 0.47 | −0.04 | 0.42 | −0.04 |

that the step-by-step annealing of thin films of RE deposited onto graphite substrates leads to the synthesis of an intercalation compound with $LaC_6$ surface stoichiometry. This stoichiometry, which relates to a $(\sqrt{3}\times\sqrt{3})R30°$ reconstruction of the crystalline structure of pristine graphite, has been found to be also characteristic for other bulk RE GIC's synthesized by a classical vapor-phase intercalation.[11,12]

The PE spectra of the samples prepared in the present study are very similar to those measured previously for La GIC.[17,20] As compared to pristine graphite, the whole electronic structure of the valence band looks shifted in RE GIC's (Fig. 1). Note particularly that the triplet structure in the region of 10 to 16 eV BE originating from $sp^2$ hybrid orbitals of graphite is maintained in the EDC's of GIC's. This demonstrates that the hexagonally arranged graphite planes are preserved in the synthesized samples. According to a series of studies of alkali-graphite intercalation compounds,[6,16,33] the shift of the valence bands in GIC's toward higher BE's causes a charge transfer from alkalies into vacant electronic states of graphite. This is achieved by the energetic lowering of the $\pi_0^*$ band, which is unoccupied in pure graphite[26] and becomes partly filled in the GIC. This band gives rise to the intense PE feature that was observed in alkali GIC's close to the Fermi energy in the region of the $K$ point.

A similar intense PE structure close to $E_F$ shows up in the EDC's of RE GIC's [Refs. 17, 18, and 20 and Figs. 1(b), 2, and 4]. However, at variance to alkali GIC's, the assignment of this structure is not straightforward in RE intercalation compounds. In contrast to alkali metals with only $s$-like valence electrons, RE elements reveal partly filled $d$ orbitals that may strongly hybridize to orbitals of carbon.

The line shape of both the Eu and the Yb $4f$ multiplets did not change throughout several hours of data acquisition, pointing to a chemical passivation of the RE ions in our samples. This fact can be well understood on the basis of the layered structure of the GIC's, where the RE atoms are incorporated into the graphite matrix and the whole system is covered by a topmost layer of graphite. A lack of $4f$ surface components in the PE spectra of Eu and Yb GIC's proves that the whole amount of deposited RE's is intercalated in the bulk.

As compared to pure RE metals, the $4f$ multiplets in Eu and Yb GIC's are shifted by 0.4 and 0.2 eV toward lower BE's, respectively. The observed negative shifts are at first sight puzzling, since by the charge transfer the RE's become positively charged and a shift to higher BE's might be expected. A corresponding shift of Ba core levels in Ba GIC that amounts to 0.6–0.7 eV was explained in terms of a hybridization between $s$ and $d$ orbitals of Ba in solids.[34] The hybridization will lead to a slight charge transfer from the Ba $6s$ into the Ba $5d$ states. Since the degree of localization is higher for $5d$ than for $6s$ orbitals, the local screening of the core potential is improved and decreasing BE's may be expected for outer shells.

This model, nevertheless, fails to explain the different core-level shifts observed in our experiments on Eu and Yb GIC's. Like barium, these two RE's have no $5d$ electrons in atomic configuration. In the GIC's as well as in the pure RE metals, in fact, some $d$ character arises due to hybridization phenomena. Yb, however, which according to our calculations reveals a larger admixture than Eu of $d$ states in GIC relative to the metallic state, shows a smaller negative core-level shift in the intercalation compound. This is even more amazing since the charge transfer from the RE to the carbon sites is larger in Eu GIC than Yb GIC (Table II).

Different shifts of the core-level emissions in Ba, Eu, and Yb GIC's relative to the pure metals can be understood within a thermochemical model,[35] which allows one to account for both initial- and final-state effects in photoemission. In this model, a Born-Haber cycle is considered, where the original process of photoexcitation is replaced by a series of thermochemical steps transforming the initial state into the photoemission final state. In particular, these steps consist of vaporization of the divalent material, photoexcitation of the RE atom in the gas phase, condensation of the excited atoms to a trivalent solid, and dissolution of the latter into the divalent host. Writing for the cohesive energy of a compound $E_{\mathrm{coh}}(\mathrm{comp})=E_{\mathrm{coh}}(\mathrm{met})-\Delta H$, where $E_{\mathrm{coh}}(\mathrm{met})$ denotes the cohesive energy of the pure metal and $\Delta H$ is the formation enthalpy of the compound, one obtains for the chemical shift $\Delta E$ (Ref. 36)

$$\Delta E=\mathrm{BE}(\mathrm{comp})-\mathrm{BE}(\mathrm{met})$$
$$=(\Delta H^{3+}-\Delta H^{2+})+[E_{\mathrm{imp}}(\mathrm{comp})-E_{\mathrm{imp}}(\mathrm{met})].$$

The first term describes the difference between the heats of formation of compounds in the trivalent and divalent states. This term is negative in most cases, since usually the presence of an additional valence electron in the trivalent configuration increases the bonding strength (note that the heat of formation is taken as negative for an exothermic process). The second term represents the difference between the heat of solution of a trivalent atom in the divalent compound and in the divalent metal (''impurity term''). This term related to the size mismatch of the final-state ion in the different chemical environment is also expected to be negative. The size-mismatch energy will generally be smaller in a compound than in a pure metal because in a compound the volume change of the RE ion may be compensated by the constituents keeping the size of the whole ''molecule'' almost unaffected. Thus, taking into account both terms, a negative value of the chemical shifts is predicted in agreement with experiment.

A quantitative estimate of the chemical shift could be obtained by using experimental values for $\Delta H$ and $E_{\mathrm{imp}}$ or by calculating these quantities by means of the semiempirical Miedema scheme.[37] Unfortunately, this scheme cannot be applied directly to divalent metals. Therefore, the chemical shifts of $4f$ emissions in Eu and Yb intercalation compounds can here only be discussed in a qualitative way. If we assume[36] that $E_{\mathrm{imp}}(\mathrm{comp})$ is small and $E_{\mathrm{imp}}(\mathrm{met})$ gives similar values for all divalent metals, then the magnitude of the chemical shift is only determined by formation enthalpies. As one may learn from Miedema's scheme, these latter quantities depend strongly on the atomic volumes and electron

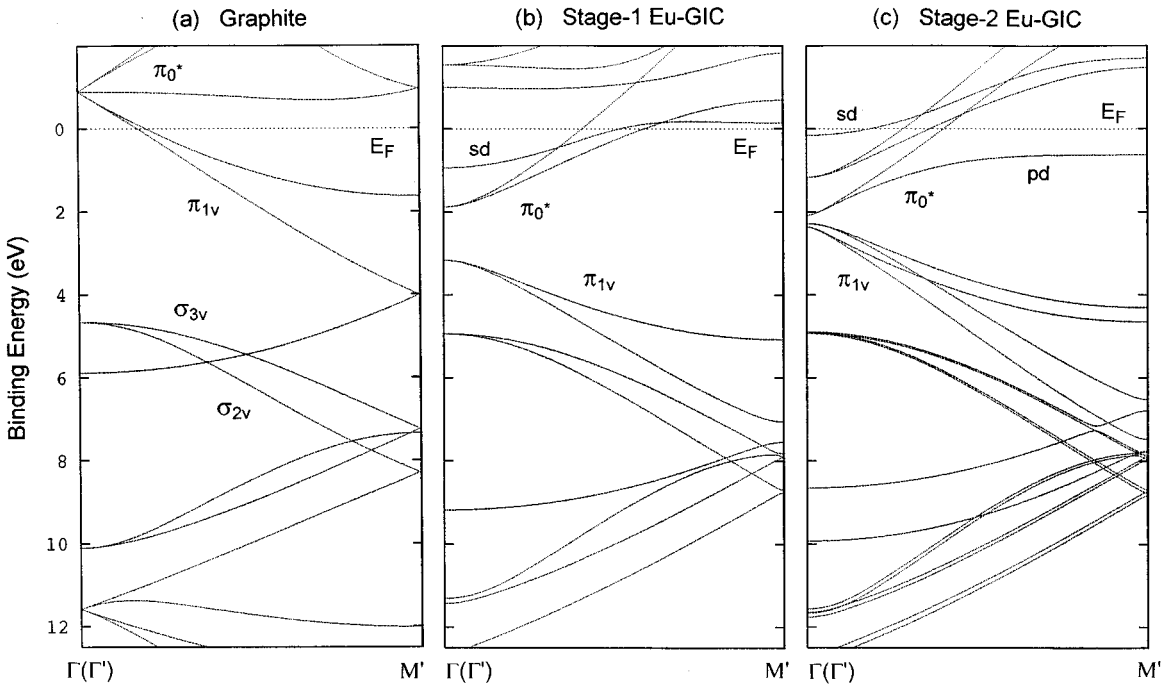


FIG. 5. Band structure along the Γ-$M'$ direction for (a) graphite with *A*-*A* stacking sequence; (b) stage-1 Eu GIC; and (c) stage-2 Eu GIC.

densities of the atoms involved. Approximating the trivalent configurations of Ba, Eu, and Yb by La, Gd, and Lu, respectively, one finds that the differences in atomic volumes and electron densities between the divalent and trivalent configurations decrease with increasing atomic number. As a consequence, the differences in the heats of formation will also decrease systematically, leading to decreasing chemical shifts in GIC's based on Ba, Eu, and Yb.

In contrast to bulk intercalation (e.g., vapor-phase method), *in situ* intercalation is restricted to incorporation of guest atoms within the first few graphite layers close to the surface. Although the $(\sqrt{3}\times\sqrt{3})R30°$ LEED pattern characteristic of RE-GIC's points to a local $REC_6$ stoichiometry, it is not easy to estimate the real bulk composition, i.e., the stage of intercalation defined by the number of graphite planes lying between neighboring RE layers.[1] On the other hand, various stages of intercalation cause different degrees of charge transfer from RE onto C atoms. According to the results of our calculations presented in Table II, the first stage of intercalation ([-RE-C-] sequence) leads to a charge transfer per C atom that is two times larger than the one for a second-stage-intercalated compound ([-RE-C-C-] sequence). This difference will be reflected by the energy position of the $\pi$-symmetry graphite-derived bands, which play the role of electron acceptors.

We have performed band-structure calculations for different sequences of RE- and graphite-derived layers. As a general trend, the results reveal a shift of the $\pi$ bands toward higher BE's with increasing RE concentration. The bands for the first- and second-stage Eu GIC's calculated along the Γ-$M'$ direction are shown in Fig. 5 in comparison to the correspondingly folded band structure of pristine graphite. In order to allow a direct comparison with the GIC's, an *A*-*A* stacking sequence[1] of the carbon planes in graphite was assumed.

The electronic structure of pristine graphite with hypothetical *A*-*A* composition, Fig. 5(a), is close to that of the real *A*-*B* stacking sequence.[26] The main differences relate to the $\pi_{1v}$ states, which are degenerated in the case of *A*-*A* assembly [Fig. 5(a)], while they are split into two bands in real-structure graphite due to the lower symmetry of the *A*-*B* crystal. A part of the $\pi_{1v}$ band around the Γ′ point lies above the Fermi energy in *A*-*A* graphite, whereas these states become filled in the case of *A*-*B* stacking. In *A*-*A* graphite, the bottom of the $\pi_{1v}$ band is located at 5.9 eV BE at the Γ point. In the Γ-$M'$ direction, this band disperses toward the Fermi energy. At the $M'$ point, the $\pi_{1v}$ band is folded back toward the Γ′ point; it then disperses upward, crossing $E_F$ at $k\cong 0.16$ Å$^{-1}$. The two $\sigma$-derived bands, which are degenerated at about 4.7 eV BE at the Γ point, move in the Γ-$M'$ direction monotonously to higher BE's. After folding at the $M'$ point, these bands continue to disperse to higher BE's when going back to the Γ point.

As can be seen in Figs. 5(b) and 5(c) the $\sigma$-derived states essentially do not change upon intercalation in either the first- or the second-stage GIC. The main differences in electronic structure of the GIC's as compared to pure graphite relate to the $\pi$-derived bands. The $\pi_{1v}$ and $\pi_0^*$ bands that are degenerated at the Γ point in graphite [Fig. 5a] are split in the first-stage GIC [Fig. 5(b)] as a result of the reduced lattice symmetry. Apart from that, these bands are almost rigidly shifted toward higher BE's; thus a part of the previously unoccupied $\pi_0^*$ band appears now below $E_F$. This supports the point[33] that the valence charge from the RE's is transferred into $p_z$ orbitals located outside the graphite planes, allowing high spatial overlap with the $spd$ orbitals of RE's. There is no evidence of a charge transfer into the interlayer band that, according to our calculations, lies above the Fermi level for both Eu and Yb GIC's.

The occupied part of the $\pi_0^*$ band contributes to the PE weight close to $E_F$, which is observed in the region of the $K(\Gamma')$ point in the EDC's presented in Figs. 1(b), 2, and 4. A similar behavior of the $\pi_0^*$ band is expected for alkali GIC's, where the corresponding Fermi-energy PE structure is also observed close to the $K$ point.[5–7]

Unlike alkali GIC's, however, RE intercalation compounds represent an additional RE-derived $sd$-hydrid band [Fig. 5(b)] located between the Fermi level and the $\pi_0^*$ band in the region of the $\Gamma$ point. This branch contains about 30% $d$ character close to the center of the BZ of Eu GIC, while in the lowest $\pi_0^*$ derived band [Fig. 5(c)] the partial contribution of $d$ symmetry considerably increases toward the BZ boundaries, reaching as much as 50% at the $M'$ point ($pd$ branch at 0.6 eV BE). Similar results were obtained for Yb GIC as well as for La GIC. These findings are in excellent agreement with our previous angle-resolved La $4d \rightarrow 4f$ resonant PE study of La GIC,[20] which reveals a stronger resonance of the Fermi-energy structure at the $M'$ point than close to the $K(\Gamma')$ point. The $d$-hybrid bands will also contribute to the PE weight close to $E_F$ in RE GIC's.

In the stage-2 GIC [Fig. 5(c)], both the $\pi_{1v}$ and $\pi_0^*$ bands are split into two subbands due to reduced symmetry of the lattice. One pair of these subbands is nearly degenerated at the $\Gamma$ point as in pure graphite, while the other pair forms a gap analogously to the stage-1 compound. This fact can be understood considering the stacking sequence [-RE-C-C-] of the stage-2 GIC that consists of two elements: [-RE-C-] and [-C-C-] characteristic of the first-stage compound and pristine graphite, respectively. The charge transfer into unoccupied C-derived states is obviously lower for a [-RE-C-C-] composition than for a [-RE-C-] configuration (Table II) and the whole structure of the $\pi$-derived bands in the stage-2 GIC's is closer to $E_F$ as compared to that in the stage-1 GIC's. Note that in the stage-2 Eu GIC, the $sd$-hybrid states are almost entirely displaced into the region of the unoccupied states. Instead, a fully occupied $pd$-symmetry branch is present in the region of the $M'$ point in this compound. The theoretically obtained charge transfer of about 0.5 electrons per RE atom in Eu and Yb GIC's is somewhat smaller than the one expected for alkali GIC's. This fact may be assigned to covalent admixtures present in RE GIC's as well as to the larger electronegativity of the RE's as compared to alkali metals. An estimate of the charge transfer on the basis of PE data is difficult. Other experimental techniques, such as NMR, might be used to check the calculated values.

An almost perfect matching of our experimental data to the band structure calculated for the stage-2 Eu and Yb GIC's indicates that compounds with [-RE-C-C-] stacking sequence were synthesized in the present study. The electronic structures of the stage-2 Eu and Yb intercalation compounds along the $\Gamma$-$M'$-$K$-$\Gamma$ high-symmetry directions are presented in Figs. 6(a) and 6(b), respectively. The experimental results are indicated by symbols of varying sizes depending on the intensity of the corresponding structure in the PE spectra. All experimental points can be assigned to theoretical branches illustrated in Fig. 6. Particularly good agreement between theory and experiment is found for both the $\pi$- and the $\sigma$-derived bands along the $\Gamma$-$M'$ direction. The results for the $\Gamma$-$K'$-$M'$ directions reveal also a reasonable

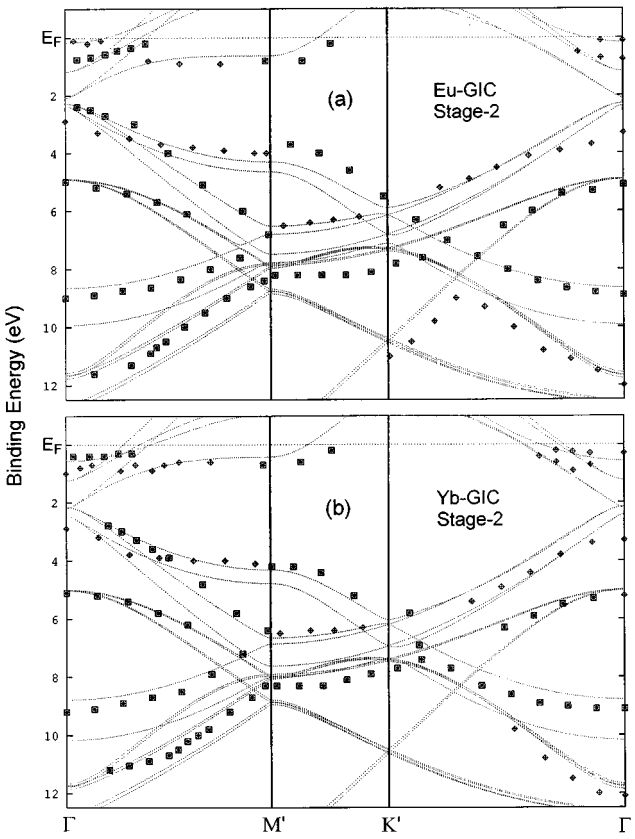


FIG. 6. Calculated electronic bands in stage-2 Eu GIC (a) and Yb GIC (b). The experimental results are indicated by symbols of different sizes. Data points corresponding to prominent PE structures (e.g., $\pi$- and $\sigma$-graphite-derived bands) are shown by large squares, while weak structures are denoted by smaller diamonds.

agreement with the theoretical predictions, while experimental points lie systematically, by 0.2–0.4 eV, lower than the calculated branches for the $\sigma$-derived bands. This effect may be related to the exact constitution of the potential that increasingly affects the calculated bands at high BE's ($\sigma$-derived branches). In the region from 1 to 2.5 eV BE, the experimental electronic structure of Eu and Yb GIC's can hardly be analyzed due to an interference of the RE $4f$-emissions in the PE spectra.

As already discussed in the preceding section, the Fermi-energy feature close to the $K$ point reveals different line shapes for Eu and Yb GIC's (Figs. 2 and 4). While in the case of the Eu GIC this structure represents a doublet with two almost equally intense PE bands [e.g., EDC taken at $\Theta = 36°$, Fig. 2(b)], it exhibits a singlet with a rather weak shoulder at the high-BE side in the PE spectra of Yb GIC [e.g., EDC taken at $\Theta = 33°$, Fig. 4(a)]. The averaged weight of the whole Fermi-energy structure appears to be shifted toward $E_F$ in Yb GIC. This behavior can be understood in the framework of our band-structure calculations. There are two bands, which contribute to the Fermi-energy structure at the $K$ ($\Gamma'$) point in Eu and Yb intercalation compounds: the $\pi_0^*$-derived branch at about 1 eV BE and the $sd$-hybrid branch located at lower BE's. There are almost no differences in the energy position of the $\pi_0^*$-derived band in both GIC's. The $sd$ hybrid in Eu GIC, however, is shifted toward

lower BE's to appear at $E_F$ in the region of the $K$ point, while this band lies fully below $E_F$ (about 0.5 eV BE) in Yb GIC. Therefore, the PE intensity of the hybrid branch is strongly reduced in Eu GIC by the Fermi-energy cutoff, while it can be fully monitored in Yb GIC as an intense line with a high-BE shoulder that stems from the $\pi_0^*$-derived band.

The observed superposition of the spectral contributions of the $\pi_0^*$ and the $sd$ hybrid bands is a main cause of the different gap values observed in Eu and Yb GIC between the maxima of the Fermi-energy structure and the PE signal from the $\pi_{1v}$ bands [Figs. 4(b) and 4(c)]. Another reason is a slight shift toward higher BE's of the averaged weight of the two $\pi_{1v}$-derived subbands in Yb GIC as compared to Eu GIC. The latter is also monitored by the results of our band-structure calculations [Figs. 5(c), 6(a), and 6(b)].

## VI. CONCLUSIONS

Our PE study on *in situ* prepared single-crystalline Eu and Yb graphite intercalation compounds shows that in analogy to alkali, alkali-earth, and La GIC's the graphite-derived valence bands are shifted toward higher BE's in GIC's as compared to pristine graphite. Additionally, an intense PE structure appears close to the Fermi energy in the EDC's of both Eu and Yb GIC's measured in the region of the $K$ ($\Gamma'$) point of the BZ. The experimental results are in excellent agreement with our LDA-LCAO band-structure calculations of stage-2 GIC's. The calculations reveal that the binding-energy shift of the graphite-derived bands causes charge transfer of approximately 0.5 valence electrons from each RE atom into vacant graphite-derived states of $\pi$ symmetry.

Qualitatively, the effect may be described by a simple rigid-band model, although such an approach cannot explain the different behavior of bands with $\pi$ and $\sigma$ symmetry. For interpretation of the Fermi-energy peaks, our more elaborate approach accounts for the hybridization between graphite-derived bands and the $5d$ states of the RE ions. The calculations show that in addition to graphite-derived states filled upon intercalation, $d$-hybrid bands also contribute to the intense Fermi-energy structure in the PE spectra of RE GIC's taken in the region of the $K(\Gamma')$ point. Apart from the $4f$ states, the electronic structure is almost identical for the Eu and Yb intercalation compounds. Minor differences relate to the amount of charge transfer and the chemical shift of the RE $4f$ emissions, both of which are larger in Eu than in Yb GIC.

In this study, stage-2 rare-earth intercalation compounds were synthesized. In principle, it might be possible to grow *in situ* RE GIC's with variable stacking sequences. Such systems could be interesting due to their quasi-two-dimensional electrical and magnetic properties.

## ACKNOWLEDGMENTS

The authors thank F. von der Decken, Graphitwerk Kropfmühl AG, München, for providing the graphite flakes. Experimental assistance by the staffs of BESSY and Universität Bochum (AG Freund) is gratefully acknowledged. Two of the authors, S.L.M. and A.M.Sh., are grateful to Technische Universität Dresden and Freie Universität Berlin, respectively, for financial support and hospitality. This work was supported by the Bundesministerium für Bildung und Forschung, BMBF, Project No. 05 625ODA 6, and by the scientific-technical program ''Fullerenes and Atomic Clusters'' of Russia.

*On leave from Institute of Physics, St. Petersburg State University, 198904 St. Petersburg, Russia.

[1] J. E. Fischer and T. E. Thompson, Phys. Today **31**, 36 (1978).
[2] *Intercalation Compounds of Graphite*, edited by F. L. Fogel and A. Herold (Elsevier Sequoia, Lausanne, 1977).
[3] *Intercalation in Layered Materials*, Volume 148 of *NATO Advanced Study Institute Series B: Physics*, edited by M. S. Dresselhaus (Plenum, New York, 1986).
[4] N. B. Hannay, T. H. Geballe, B. T. Matthias, K. Andres, P. Schmidt, and D. MacNair, Phys. Rev. Lett. **14**, 225 (1965).
[5] W. Eberhardt, I. T. McGovern, E. W. Plummer, and J. E. Fischer, Phys. Rev. Lett. **44**, 200 (1980).
[6] N. Gunasekara, T. Takahashi, F. Maeda, T. Sagawa, and H. Suematsu, Z. Phys. B **70**, 349 (1988).
[7] C. Fretigny, D. Marchand, and M. Laguës, Phys. Rev. B **32**, 8462 (1985).
[8] Th. Fauster, F. J. Himpsel, J. E. Fischer, and E. W. Plummer, Phys. Rev. Lett. **51**, 430 (1983).
[9] D. Anselmetti, R. Wiesendanger, and H.-J. Güntherodt, Phys. Rev. B **39**, 11 135 (1989).
[10] D. Anselmetti, V. Geiser, G. Overney, R. Wiesendanger, and H.-J. Güntherodt, Phys. Rev. B **42**, 1848 (1990).
[11] G. Kaindl, J. Feldhaus, U. Ladewig, and K. H. Frank, Phys. Rev. Lett. **50**, 123 (1983).
[12] M. El Makrini, D. Guerard, Ph. Lagrange, and A. Herold, Physica **99B**, 481 (1980).
[13] R. K. Mittleman, Phys. Rev. B **36**, 6001 (1987).
[14] W. Schülke, A. Berthold, H. Schulte-Schrepping, K.-J. Gabriel, V. Thommes-Geiser, and H.-J. Güntherodt, Solid State Commun. **79**, 661 (1991).
[15] T. Inoshita, K. Nakao, and H. Kamimura, J. Phys. Soc. Jpn. **43**, 1237 (1977).
[16] N. A. W. Holzwarth, S. G. Louei, and S. Rabii, Phys. Rev. B **30**, 2219 (1984).
[17] A. M. Shikin, S. L. Molodtsov, C. Laubschat, G. Kaindl, G. V. Prudnikova, and V. K. Adamchuk, Phys. Rev. B **51**, 13 586 (1995).
[18] A. M. Shikin, G. V. Prudnikova, V. K. Adamchuk, S. L. Molodtsov, C. Laubschat, and G. Kaindl, Surf. Sci. **331-333**, 517 (1995).
[19] G. V. Prudnikova, A. G. Vjatkin, A. V. Ermakov, A. M. Shikin, and V. K. Adamchuk, J. Electron. Spectrosc. Relat. Phenom. **68**, 427 (1994).
[20] S. L. Molodtsov, Th. Gantz, C. Laubschat, A. G. Viatkine, J. Avila, C. Casado, and M. C. Asensio, Z. Phys. B **100**, 381 (1996).
[21] M. Posternak, A. Baldereschi, A. J. Freeman, E. Wimmer, and M. Weinert, Phys. Rev. Lett. **50**, 761 (1983).
[22] L. Hedin and B. I. Lundqvist, J. Phys. C **4**, 2064 (1971).
[23] H. Eschrig, *Optimized LCAO Method* (Springer, Berlin, 1989).
[24] M. Richter and H. Eschrig, Solid State Commun. **53**, 529 (1989).

[25] H. J. F. Jansen and A. J. Freeman, Phys. Rev. B **35**, 8207 (1987).
[26] R. Ahuja, S. Auluck, J. Trygg, J. M. Wills, O. Eriksson, and B. Johansson, Phys. Rev. B **51**, 4813 (1995).
[27] A. R. Law, J. J. Bary, and H. P. Hughes, Phys. Rev. B **28**, 5332 (1983).
[28] A. Bianconi, S. B. Hagström, and R. Z. Bachrach, Phys. Rev. B **16**, 5543 (1977).
[29] E. Dietz and D. E. Eastman, Phys. Rev. Lett. **41**, 1674 (1978).
[30] A. R. Law, M. T. Johnson, and H. P. Hughes, Phys. Rev. B **34**, 4289 (1986).
[31] C. G. Olson, X. Wu, Z.-L. Chen, and D. W. Lynch, Phys. Rev. Lett. **74**, 992 (1995).
[32] J. Avila, A. G. Vjatkin, M. C. Asensio, S. L. Molodtsov, Th. Gantz, and C. Laubschat (unpublished).
[33] D. P. DiVincenzo and S. Rabii, Phys. Rev. B **25**, 4110 (1982).
[34] M. E. Preil, J. E. Fischer, S. B. DiCenzo, and G. K. Wertheim, Phys. Rev. B **30**, 3536 (1984).
[35] B. Johansson, Phys. Rev. B **20**, 1315 (1979).
[36] C. Laubschat, G. Kaindl, W. D. Schneider, B. Reihl, and N. Mårtensson, Phys. Rev. B **33**, 6675 (1986).
[37] A. R. Miedema, Z. Metallkd. **69**, 456 (1978).